EPJ Web of Conferences **40**, 15005 (2013)
DOI: 10.1051/epjconf/20134015005

Charge compensation and magnetic properties in Sr and Cu doped La-Fe perovskites

I. Natali Sora [1], T. Caronna [1], F. Fontana [1], C. de Julián Fernández [2,3], A. Caneschi [3], M.A. Green [4,5], and P. Bonville [6]

[1]INSTM R.U. and Department of Engineering, University of Bergamo, Dalmine, BG, I-24044 Italy
[2]CNR - Istituto di Scienze e Tecnologie Molecolari (ISTM), 20133 Milano, Italy
[3]INSTM R.U. Firenze and Department of Chemistry, University of Florence, I-50019 Sesto Fiorentino, Italy
[4]Center for Neutron Research, NIST, Gaithersburg, MD, USA
[5]Department of Materials Science and Engineering, University of Maryland, College Park, MD20742-2115, USA
[6]CEA, Centre de Saclay, Service de Physique de l'Etat Condensé, 91191 Gif-sur-Yvette, France.

Abstract. Orthorhombic lanthanum orthoferrites $La_{0.8}Sr_{0.2}Fe_{1-y}Cu_yO_{3-w}$ (y = 0 and 0.10) have been studied using X-rays and neutron powder diffraction (XRPD and NPD), magnetization measurements and ^{57}Fe Mössbauer spectroscopy. Rietveld refinements on XRPD and NPD data show that they adopt an orthorhombic ABO_3 perovskite symmetry with La/Sr and Fe/Cu atoms randomly distributed on crystal A and B sites, respectively. The magnetic structure at room temperature is antiferromagnetic, with the Fe/Cu magnetic moments aligned along the a axis. Magnetization curves versus temperature show that the compounds exhibit an overall antiferromagnetic and a weak ferromagnetic behaviour in the range 5-298 K. ^{57}Fe Mössbauer spectroscopy measurements indicate that Fe^{3+} and Fe^{5+} ions coexist in both compounds, and the relative percentage of Fe^{5+} is almost the same at 77 and 170 K, rejecting a charge disproportion mechanism.

1 Introduction

Lanthanum orthoferrite $LaFeO_3$, with perovskite structure, exhibits important and varied properties (catalytic, electrical, magnetic, etc.) together with chemical and thermal stability. Doped lanthanum ferrites are widely studied for use in catalysis [1-4], as cathode materials for solid oxide fuel cells (SOFCs) [5-8] and in chemical sensors applications [9-10]. Dann et al [11] studied the $La_{1-x}Sr_xFeO_{3-w}$ system using neutron powder diffraction measurements and Mössbauer spectroscopy. They found that in $La_{0.8}Sr_{0.2}FeO_{3-w}$ full oxygen stoichiometry is maintained (w = 0) and the crystal symmetry of the compound is orthorhombic. Mössbauer spectra collected in the temperature range 4.2 K to 298 K showed that in $La_{0.8}Sr_{0.2}FeO_{3-w}$ the charge states Fe^{3+} and Fe^{5+} coexist. In general these perovkites exhibit a wide variety of magnetic phenomena, due to the presence of different competitive antiferromagnetic interactions modified by the effects of charge ordering and disproportion [12]. Whilst the charge disproportion of Fe^{4+} and concomitant Fe^{3+}- Fe^{5+} charge ordering below its Néel temperature of ~ 200 K is well-documented in literature for higher Sr doping (x = 2/3) (*e.g.* [12] and [13] and references cited), information on Fe^{4+} formation in $La_{0.8}Sr_{0.2}FeO_{3-w}$ compound is lacking. When doping with metals $La_{0.8}Sr_{0.2}Fe_{1-y}M_yO_{3-w}$ oxides, where M is a transition-metal atom, the Sr atom influences the physical properties mainly through steric effects whereas the transition-metal M atom plays an important role by way of its electronic ground state (charge state and spin) and its magnetic properties. The most recent structural and magnetic study performed on $La_{0.8}Sr_{0.2}Fe_{1-y}Cu_yO_{3-w}$ was by Natali Sora et. al [14] using neutron powder diffraction technique. At room temperature, the magnetic structure was successfully modelled for y = 0.05 and 0.10 assuming an antiferromagnetic interaction between Fe/Cu neighbouring cations (G-type), and magnetic moments were calculated. Moreover, at room temperature the oxides exhibit high coercive fields and irreversibility fields that are larger than any other reported for iron-based perovskites.

The objective of this work is to investigate more deeply the complex magnetic behaviour of the $La_{0.8}Sr_{0.2}Fe_{1-y}Cu_yO_{3-w}$ system at low values of Cu substitution, and to attempt a correlation with the structural and chemical features and the experimentally determined Mössbauer parameters.

2 Experimental

Nanosized powders of $La_{0.8}Sr_{0.2}FeO_{3-w}$ (LSF20) and $La_{0.8}Sr_{0.2}Fe_{0.9}Cu_{0.1}O_{3-w}$ (LSFC2010) were prepared by citrate auto-combustion of dry gel obtained from a

solution of corresponding nitrates into citric acid solution [14-15]. The powders were calcined at 1253 K in air for 3 h. For both compounds powder X-ray diffraction patterns were collected at room temperature (Bruker D8 Advance diffractometer), in the 2θ range 5 - 90°, using Cu-K_α radiation; the step scan was 0.02° 2θ and the counting time of 10 s per step. For LSFC2010 also neutron powder diffraction data were collected and the experimental details have been previously reported [14]. The structural refinements were carried out with the Rietveld method of profile analysis.

Magnetization measurements as a function of temperature and applied magnetic field were performed using a SQUID magnetometer that reaches the maximum field of 5 T. Mössbauer absorption spectra on the isotope ^{57}Fe have been carried out at 77 K in LSF20 and LSFC2010, and 170 K for LSFC2010.

3 Results and discussion

The structural refinements using the Rietveld method of profile analysis were performed on room temperature X-rays and neutron powder diffraction (XRPD and NPD) data, and the most important results are reported in Table 1. LSF20 and LSFC2010 powders were monophasic with *Pnma* orthorhombic symmetry, and crystallize in the perovskite-like cell of $LaFeO_3$, with Fe/Cu cations occupying octahedral sites. For LSFC2010 oxygen content determined by NPD resulted in full occupancy of the oxygen sites. The unit cell volume decreases with Cu doping. Since the larger Cu^{2+} cation partially substitutes the Fe^{3+} cation (Cu^{2+}(VI) = 0.73 Å, Fe^{3+}(VI) = 0.645 Å), a charge compensation mechanism occurs by oxidation of Fe/Cu cations. Hence several charge states Fe^{3+}- Fe^{4+} - $Fe^{5+}$and Cu^{2+}- Cu^{3+} of different magnetic properties are possible.

Table 1. Selected experimental results from XRPD study (LSF20) and NPD study (LSFC2010).

	LSF20 from XRPD	**LSFC2010 from NPD**
Space group	*Pnma*	*Pnma*
a (Å)	5.5287(3)	5.51440(8)
b (Å)	7.8214(5)	7.81033(12)
c (Å)	5.5543(3)	5.54705(8)
V(Å^3)	240.18(2)	238.908(6)
Fe/Cu-O(1) (Å)	1.997(7) x2	1.9848(6) x2
Fe/Cu-O(2) (Å)	1.96(5) x2	1.977(2) x2
Fe/Cu-O(2) (Å)	1.99(5) x2	1.979(2) x2
Average (Å)	*1.98*	*1.980*
Fe/Cu-O(1)-Fe/Cu (deg)	156.6(5)	159.3(2)
Fe/Cu-O(2)-Fe/Cu (deg)	166.7(7)	162.7(1)

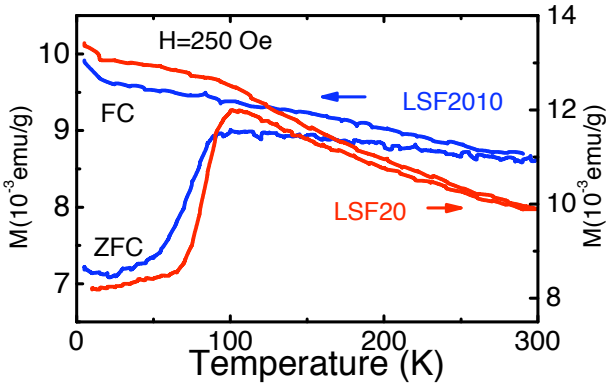

Fig. 1. ZFC and FC magnetization versus temperature at 250 Oe magnetic field for LSF20 and LSFC2010. Curves are scaled to better see the differences.

In the neutron diffraction patterns additional peaks in the low angle region were present resulting in additional magnetic scattering. The magnetic peaks could be indexed based on the nuclear unit cell. The magnetic structure was modelled only for LSFC2010 assuming an antiferromagnetic interaction between Fe/Cu neighbouring cations (G-type), with the moments aligned along the *a* axis. The magnetic moment of the Fe/Cu atoms is $\mu_x = 2.43(3)\mu_B$ for LSFC2010.

The magnetic properties were further investigated by measuring the magnetization as a function of temperature (in the range 5-300 K) and applied magnetic field. Figure 1 shows the Zero-Field-Cooled (ZFC) and Field-Cooled (FC) magnetization *versus* temperature for LSF20 and LSFC2010 measured applying a field of H = 250 Oe. The ZFC curves of both samples exhibit similar temperature dependence: the magnetization is almost constant from low temperature to 60-70 K, above which the magnetisation increases reaching the maximum at 90-100 K, and at higher temperature the magnetization decreases continuously. On the other hand the FC magnetizations decrease continuously as the temperature increases. These results indicate in a first instance a change of the magnetic behaviour around the inflexion temperature of T_s = 80 K and 70 K (T_s, the temperature at which the increment is larger) for LSF20 and LSFC2010, respectively.

The study described in ref. [14] reports that the oxides LSF20 and LSFC2010 exhibit a weak ferromagnetic behaviour at room temperature. It is reasonable to hypothesize that the jump of the magnetization curve in the temperature dependence diagram could be due to a Morin-like transition from a room temperature weak ferromagnetism to a low temperature antiferromagnetism. Hence the low temperature behaviour was investigated. Figure 2 shows the magnetization versus applied magnetic field at 5 K, well below T_s. The hysteresis loops of both samples are open and exhibit irreversibility even at the maximum applied field of 50 kOe. The saturation of the magnetization is never reached. The coercive fields, H_c,

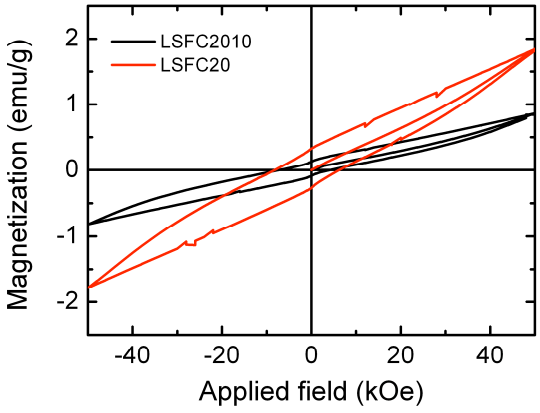

Fig. 2. Hysteresis loops measured at the temperature of 5 K.

are 8 kOe and 7 kOe respectively for LSF20 and LSFC2010. These results indicate that the magnetic behaviour below T_s is also characterized by a weak ferromagnetic order, so a low temperature Morin-like transition can be excluded.

The magnetization versus temperature was also measured by applying the maximum available magnetic field of 5 T, the magnetization curves were similar to those illustrated in Figure 1. Figure 3 shows the remanence ZFC (rZFC) and FC magnetizations *versus* temperature. In the rZFC magnetization, the sample is cooled in zero-field after the application of 5 T magnetic field at room temperature. As well as in Figure 1 the jump is observed only in rZFC curves, although the oxides are magnetized (in the remanence state), and not for FC measurements. In both samples the rZFC curves show a transition with T_s = 95 K what implies an increase of the T_s respect to the low field measurement. Also the percentage of the increment of the magnetization in the jump applying 50 kOe is slightly smaller, 25%, the increment obtained applying low fields, 30-40%. These results suggest that magnetic field drives the properties at the transition, hence charge ordering effects correlated to charge disproportion mechanism can be considered.

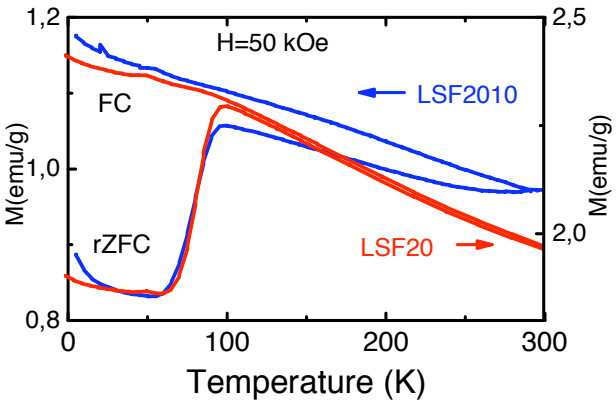

Fig. 3. Remanence ZFC (rZFC) and FC magnetization versus temperature at 50 kOe magnetic field for LSF20 and LSFC2010. Curves are scaled to better see the differences.

In order to further investigate the nature of the magnetic transition the existence of a low temperature charge disproportion mechanism was examined by Mössbauer spectroscopy at different temperatures. Mössbauer absorption spectra on the isotope ^{57}Fe have been carried out at 77 K in LSF20 and LSFC2010, and 170 K for LSFC2010. In both compounds, the 77 K spectra consist in three subspectra, two clearly corresponding to Fe^{3+} (Isomer Shift w.r. to α-Fe close to 0.45 mm/s, hyperfine field above 50 T) and the third to a Fe valence state with I.S. close to -0.1 mm/s and hyperfine field 26 T. This latter state, according to Ref. [11], can be attributed to Fe^{5+}. In the Figure 4 the blue and green subspectra correspond to Fe^{3+}, the red one to Fe^{5+}. Hyperfine parameters and relative weights of the subspectra in both samples are given in the Table 2. The linewidths of the sub-spectrum with hyperfine field 53 T (green) are systematically larger than those of the other subspectra. The error bars on the parameters are small due to the good statistics of the spectra: those on the relative percentages can be estimated to ±1%. With respect to the fit of the spectra at 77 K, the Mössbauer spectrum obtained at 170 K was adequately fitted adding a small Fe^{3+} doublet (1.5%), the origin of which is unknown, which accounts for the peak near zero velocity. The doublet is also visible at 77 K, but to a lesser extent.

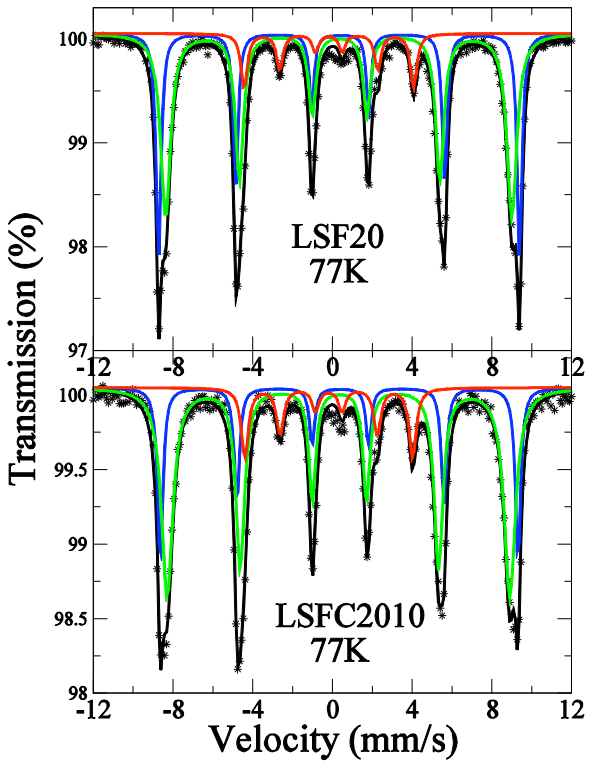

Fig. 4. Mössbauer spectra for LSF20 and LSF2010 collected at 77 K.

Table 2. Parameters obtained from the Mössbauer spectra collected at 77 K and 170 K.

Samples	I. S. (mm/s)/ α-Fe	Hyperfine field (T)	Relative %	Charge state
LSF20 at 77 K	0.47	56.0	34	Fe^{3+}
	0.44	53.8	55	Fe^{3+}
	-0.07	26.3	11	Fe^{5+}
LSFC2010 at 77 K	0.47	55.5	24	Fe^{3+}
	0.43	53.2	63	Fe^{3+}
	-0.073	26.1	13	Fe^{5+}
LSFC2010 at 170 K	0.45	54.7	24	Fe^{3+}
	0.41	52.2	62	Fe^{3+}
	-0.06	25.2	12.5	Fe^{5+}
	0.41	-	1.5	Fe^{3+}

The Mössbauer results indicate: (*i*) the presence of two sextets with isomer shifts corresponding to Fe^{3+}, (*ii*) the presence of one sextet with isomer shift corresponding to Fe^{5+}, (*iii*) hyperfine parameters typical of Fe^{3+} and Fe^{5+} ions with octahedral coordination, (*iv*) the relative percentage of the two Fe^{3+} is different for different compositions, while Fe^{5+} poorly increases with the Cu content, and (*v*) while no structure related to Fe^{4+} is observed, above and below T_s, the amount of Fe^{3+} and Fe^{5+} does not vary. These data exclude charge disproportion for LSFC2010 in the range 77-170 K.

4 Conclusions

The coexistence of antiferromagnetic and weak ferromagnetic behavior at room temperature was determined by NPD and the magnetic hysteresis loop, respectively. The room temperature magnetic moment of the Fe/Cu atoms is $\mu_x = 2.43(3)\mu_B$ for LSFC2010. In addition, the nanosized LSF20 and LSFC2010 powders exhibit an interesting low temperature jump (at 70-80 K) in the ZFC magnetization curves versus temperature. In order to elucidate their complex magnetic behavior several hypotheses have been investigated: (*i*) magnetic hysteresis loops at 5 K excluded a Morin-like transition from a room temperature weak ferromagnetism to a low temperature antiferromagnetism; (*ii*) ^{57}Fe Mössbauer spectroscopy measurements indicated that Fe^{3+} and Fe^{5+} ions coexist in both compounds, but the relative percentage of Fe^{5+} is almost the same at 77 and 170 K, rejecting a charge disproportion mechanism Further work will be required to ascertain whether a low temperature structural transition takes place, and to investigate a possible size effect on magnetic behavior.

References

1. J. Pérez-Ramìez, B. Vigeland, Catal. Today. **105**, 436 (2005)
2. V.A. Sadykov, L.A. Isupova, I.S. Yakovleva, G.M. Alikina, A.I. Lukashevich, S. Neophytides, React. Kinet. Catal. Lett. **2**, 393 (2004)
3. D. Mescia, J.C. Caroca, N. Russo, N. Labhsetwar, D. Fino, G. Saracco, V. Specchia, Catal. Today. **137**, 300 (2008)
4. S. Furfori, S. Bensaid, N. Russo, D. Fino, Chem. Eng. J. **154**, 348 (2009)
5. H. Kishimoto, N. Sakai, T. Horita, K. Yamaji, M.E. Brito, H. Yokokawa, Solid State Ionics. **178**, 1317 (2007)
6. D. Burnat, P. Ried, P. Holtappels, A. Heel, T. Graule, D. Kata, Fuel Cells. **10**, 156 (2010)
7. L. T. Wilkinson, J. H. Zhu, J. Electrochem. Soc. **156**, 905 (2009)
8. J.S. Yoon, J. Lee, H.J. Hwang, C.M. Whang, J. Moon, D. Kim, J. Power Sources. **181**, 281 (2008)
9. J. Wang, F. Wu, G. Song, N. Wu, J. Wang, Ferroelectrics **323**, 71 (2005)
10. A. Cavalieri, T. Caronna, I. Natali Sora, J.M. Tulliani, Ceramics International, **38**, 2865 (2012)
11. Dann, S. E.; Currie, D.B.; Weller, M.T. J. Solid State Chem. **109**, 134 (1994)
12. H. Kong, C. Zhu, Appl. Phys. Lett. **88**, 041920 (2006)
13. SK. Park, T. Ishikawa, Y. Tokura, JQ Li, Y. Matsui, Phys. Rev. B **60** 10788 (1999)
14. I. Natali Sora, T. Caronna, F. Fontana, C. De Julián Fernández, A. Caneschi, M. Green, J. Solid State Chem. **191**, 33 (2012)
15. T. Caronna, F. Fontana, I. Natali Sora, R. Pelosato, Mater. Chem. Phys. **116**, 645 (2009)